Appl. Phys. A (2017) 123:77
DOI 10.1007/s00339-016-0711-6

Applied Physics A
Materials Science & Processing

Perfect absorbers based on metal–insulator–metal structures in the visible region: a simple approach for practical applications

G. Kenanakis[1] · Ch. P. Mavidis[1,2] · E. Vasilaki[3] · N. Katsarakis[1,4] · M. Kafesaki[1,2] · E. N. Economou[1] · C. M. Soukoulis[1,5]

Received: 10 October 2016 / Accepted: 15 December 2016 / Published online: 23 December 2016

Abstract Perfect absorbers based on metal–insulator–metal (MIM) structures are proposed and demonstrated, both theoretically and experimentally, in the visible region. The proposed structures may possess either sharp or broadband absorption peaks, by simply choosing a single layer of the proposed MIM structure or building several layers of them, while no nanofabrication steps or structure patterning are required, and thus can be easily made to cover a large area. The highly efficient absorption of the MIM structures is maintained for both TE and TM incident polarization, and for angles of incidence up to 75°, indicating that the proposed perfect absorbers can be potentially deployed for solar cells applications and optics.

1 Introduction

During the last decade, broadband perfect electromagnetic (EM) wave absorbers have been widely investigated from radio to optical frequencies, since they can find numerous applications [1, 2], such as photovoltaic [3] and thermophotovoltaic energy conversion [4, 5], thermal imaging [6] and electromagnetic shielding [2], to name but a few.

Recently, broadband perfect absorbers have been realized by utilizing metal–dielectric stacks with certain patterned structures [1, 4, 5]. Typically, these absorbers consist of a lossy dielectric layer on top of a metal ground plane, while a top metal layer can be patterned using nanolithography methods to selectively tune the absorption or the thermal emission properties of the structure [4]. A main drawback of such perfect absorbers is that nanofabrication techniques are essential in order to build the structures, for example electron-beam lithography used in commercial applications which is highly expensive, or even nanoimprint lithography which is a low-cost technique with several disadvantages, such as surface sticking and thermal expansion issues [7]. Moreover, one typical problem of such absorption systems based on nanosized patterned metallic structures is their sensitivity to polarization and/or angle of incidence of the incoming EM field. Usually, the perfect absorption is preserved only for a small incidence angle range, or for a certain polarization [8]; moreover, most of the absorbers discussed in the literature are quite narrowband, as a result of the resonance origin of the high absorption [9, 10].

In this work, a type of light absorber made of continuous layers of metal and dielectric films is studied both theoretically and experimentally, following the approach of Yan [11] and Kajtár et al. [12]. In this case, geometric resonances induced by multiple reflections in the structure, when combined with the inherent lossy nature of metals, result in spectral regions of strong absorption [2]. We demonstrate theoretically and experimentally a perfectly absorbing metal–insulator–metal (MIM) structure, fabricated using quite simple and inexpensive techniques such

✉ G. Kenanakis
gkenanak@iesl.forth.gr

[1] Institute of Electronic Structure and Laser, Foundation for Research and Technology-Hellas, N. Plastira 100, 700 13 Heraklion, Crete, Greece

[2] Department of Materials Science and Technology, University of Crete, 710 03 Heraklion, Crete, Greece

[3] Department of Chemistry, University of Crete, 710 03 Heraklion, Crete, Greece

[4] Electrical Engineering Department, School of Engineering, Technological Educational Institute of Crete, Heraklion, Greece

[5] Ames Laboratory-USDOE, and Department of Physics and Astronomy, Iowa State University, Ames, IA 50011, USA

as thermal evaporation and sol–gel/spin coating, which avoids the above-mentioned angle and polarization restrictions, while it can be easily extended to give multi-band and broadband absorption.

2 The structures and investigation approach

In the simplest configuration, the MIM structure consists of two metallic layers separated by a dielectric spacer sheet, in which the bottom metallic film is electromagnetically thick in order to minimize light transmission. One representative geometry, along with the dimensions of the MIM structure fabricated in this work, is schematically shown in Fig. 1.

In the samples presented in Fig. 1, the gold films were evaporated on standard 10 × 10 mm^2 Corning Eagle 2000 Borosilicate Glass (Specialty Glass Products) substrates from a ceramic source at 1100 °C using a commercial NormVac Thermal evaporator, with a deposition rate of about 0.5 Å/s.

TiO_2 thin films with a thickness of 150 nm were deposited on gold-covered glass substrates using a sol–gel/spin coating technique. In particular, 2.8 ml of $Ti(OCH(CH_3)_2)_4$ was first dissolved in 25 ml of absolute ethanol. The resultant solution was stirred for 15 min at 60 °C using a magnetic stirrer to yield a homogeneous, clear and transparent solution. Five drops of concentrated hydrochloric acid were added in order to get an acidic solution, as proposed by Rampaul et al. [13] and Kenanakis et al. [14], and avoid precipitation (changing the pH value of the precursor solution from ~8.5–9.0 to ~1.25–1.75). The deposition was usually performed within 24 h after the solution was prepared, by spin coating the substrates at 3000 rpm for 20 s. After processing, the substrates were heated at 350 °C for 10 min to evaporate the solvent and remove the organic residuals from the films. This procedure was repeated up to 4 times. The films were then annealed in air at 600 °C for 120 min. The thickness of the films was measured using a stylus profilometer (alpha-step 100, Tencor).

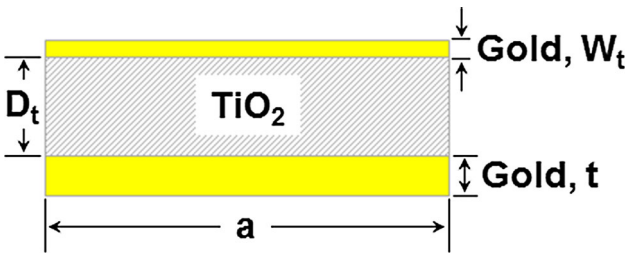

Fig. 1 MIM-based absorber structure, under investigation. *Yellow* corresponds to noble metal (gold in our case); *gray* to dielectric spacer (TiO_2). The geometrical features of the MIM structures are: $t = 150$ nm, $D_t = 150$ nm, and $W_t = 20$ nm, respectively

Before deposition, the glass substrates were cleaned for 10 min using a piranha solution ($H_2SO_4/H_2O_2 = 3/1$), rinsed with ultrapure water (18.2 MΩ cm) and dried under N_2 gas flow [14].

The crystal structure of the TiO_2 films was determined by X-ray diffraction (XRD) using a Rigaku (RINT 2000) diffractometer with Cu *Ka* X-rays, while their surface morphology was studied by means of a field emission scanning electron microscope (FE-SEM, JEOL JSM-7000F) and an atomic force microscope (AFM) in tapping mode (Digital Instruments—Nanoscope IIIa).

The experimental EM characterization of the MIM-based absorber structures (see Fig. 1) was performed in the frequency regime 450–1200 nm through transmission and reflection measurements, using a Bruker Vertex 70v Fourier transform infrared spectrometer (with a collimated beam), equipped with a room-temperature triglycine sulfate (DTGS) detector and two fused silica ultra-broadband linear wire grid polarizers.

The results of the measurements were compared in all cases with corresponding simulations. For the simulations, we used a commercial three-dimensional full-wave solver (CST Microwave Studio, Computer Simulation Technology GmbH, Darmstadt, Germany) based on the finite element method. We considered in the simulations a single unit cell, as shown in Fig. 1, with periodic boundary conditions in lateral directions. For modeling the metallic parts of the structure (gold; yellow color in Fig. 1), we considered experimental data by Johnson and Cristy [15], while for the TiO_2 areas (marked in gray in Fig. 1) we used experimental data obtained from Palik [16].

3 Results and discussion

As already stated in our previous work [14], the 150-nm-thick TiO_2 thin films fabricated following a sol–gel/spin-coating approach exhibited all the X-ray diffraction peaks (25.34°, 37.84°, 48.18°, 54.02° and 55.12°), in good agreement with the JCPDS card (No. 84-1286) for the crystal structure of anatase [13, 14, 17–21].

The surface morphology of the dielectric films presented in Fig. 1, which was studied by means of AFM and SEM analysis (not shown here), revealed that TiO_2 thin films are homogeneous, crack-free and densely packed, while their grains are significantly small, exhibiting values of 22 ± 4 nm and a rout-mean-square (RMS) surface roughness of ~1.8 nm [14].

In Fig. 2a, one can see the absorption (blue line), transmission (red line) and reflection (green line) spectra based on theoretical calculations for normal incidence,

while Fig. 2b depicts the comparison between theoretical (blue solid line) and experimental (black dotted line) absorption spectra of the MIM-based absorber structure under investigation.

As evident from Fig. 2, the transmission is predominantly close to zero across the examined spectral range (red line in Fig. 2a). Thus, the bottom 150-nm-thick gold film can be treated as optically opaque throughout this work. The thickness of the bottom gold film is not very critical for the purpose addressed in this work (i.e., for achieving maximum absorption), as soon as it is quite larger than the metal skin depth, as to ensure transmission close to zero.

The effect of the thickness of the top gold layer on the structure's absorbance spectrum was also studied theoretically. For the case without the top gold layer, the MIM structure becomes a gold mirror coated with a spacer layer; therefore, most of the incident light is reflected back with little absorption, and resonant behavior is not observed, while as the thickness of the top gold layer increases (up to a critical thickness) the absorption becomes higher with distinguished peaks and dips due to the resulted Fabry–Perot resonant cavity formed between the two metallic layers [22–24].

One main advantage of the proposed MIM structure is that one can tune the frequency of the absorption peaks by changing the thickness of the TiO_2 dielectric spacer. For example, Fig. 3a illustrates the thickness of the dielectric spacer needed in order to get absorption peaks higher than 90% (for top metal layer thickness 20 nm). Moreover, in Fig. 3a one can notice the shift of the absorption peaks to longer wavelengths, as the TiO_2 spacer increases [12], as expected from features originated from Fabry–Perot resonances. Finally, the full width at half maximum (FWHM) of the absorption peaks can be tuned, depending on the desired application. Figure 3b illustrates FWHM of the absorption peaks varying from 10 to 100 nm. For example, one can notice from Fig. 3b that the absorption peak centered at ~550 nm can be quite sharp (processing a FWHM of ~10 nm), or relatively broad (FWHM ~100 nm), by simply changing the thickness of the TiO_2 layer from 175–475 to 25–50 nm, respectively.

Since, as already stated, the structures of Fig. 1 are essentially proposed as broadband perfect absorbers, their high absorption ought to be maintained for any incident wave polarization. In Fig. 4, the theoretical absorption spectra are shown for different angles of incidence [0°, 15°, 30°, 45°, 60° and 75° for TM—the magnetic field vector being parallel to the surface (Fig. 4a)—and TE—the electric field vector being parallel to the surface (Fig. 4b)—polarized incident waves] for the structure of Fig. 1.

Obviously, in Fig. 2a, b, because of the normal incidence and the flat property of the geometry, this MIM perfect absorber performs exactly the same for TM polarization (with magnetic field perpendicular to the wave vectors plane) and TE polarization (with the electric field perpendicular to the wave vectors plane). When the incident angle increases from zero, the absorption peak displays a noticeable wavelength shift but still has nearly perfect absorption efficiency for both polarizations, as shown in Fig. 4.

We note that the nearly perfect absorption behaviors are almost the same within an angular incidence of up to 30° for both polarizations, while the resonant peak positions of the MIM structures were slightly blue shifted (Fig. 4a, b). If the incident angle is further increased to 75°, the absorption peaks of the MIM structure are reduced and both absorption peaks shift to lower wavelengths for TE and TM polarizations.

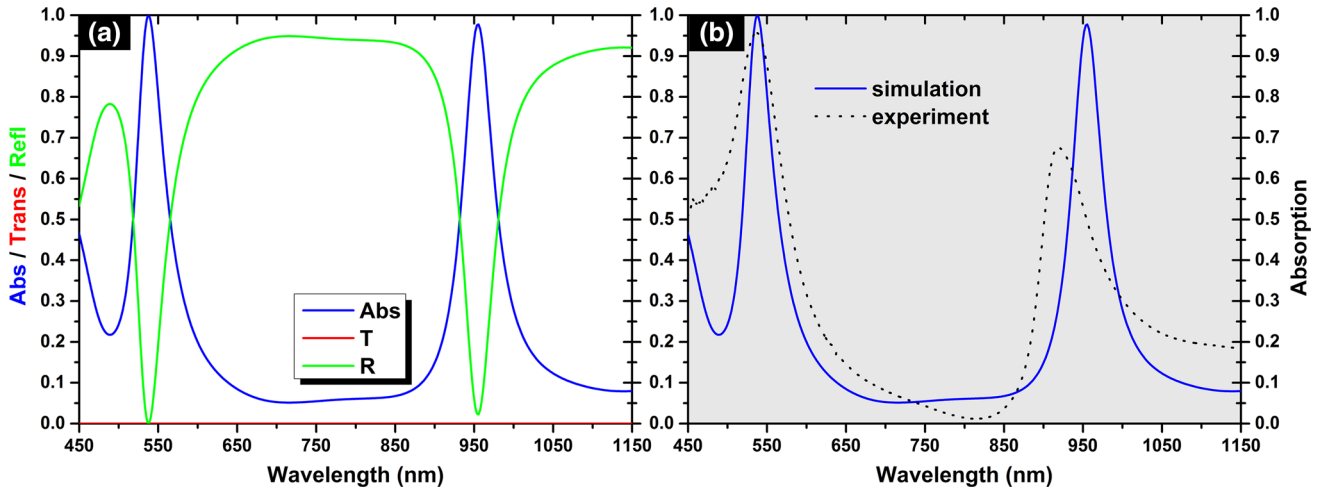

Fig. 2 Absorption (*blue line*), transmission (*red line*) and reflection (*green line*) spectra based on simulations for normally incident EM wave (**a**), and comparison between theoretical (*blue solid line*) and experimental (*black dotted line*) absorption spectra of the MIM-based absorber structure under investigation (**b**)

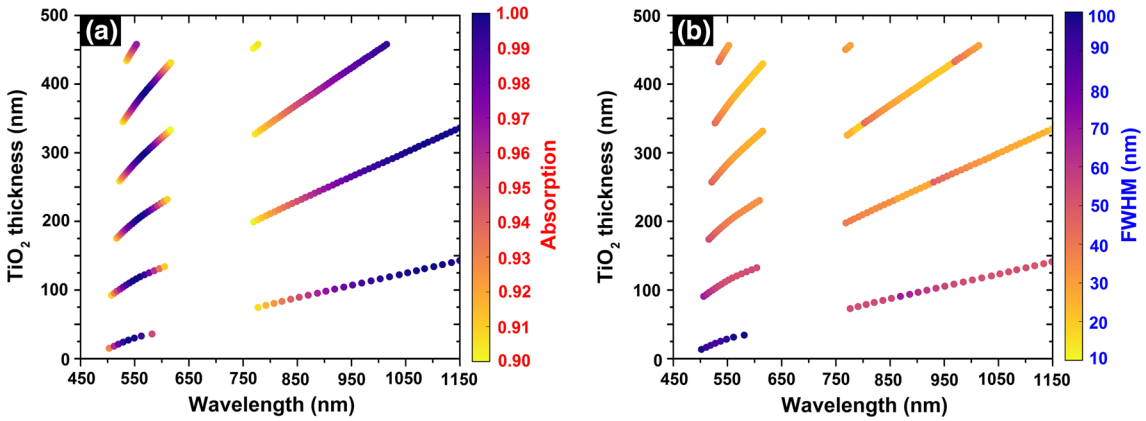

Fig. 3 Simulations indicating the desirable thickness of TiO_2 dielectric layer as a function of the wavelength for absorption to occur at a level higher than 90% (**a**), and FWHM of the absorption peaks with intensity higher than 90% (**b**), respectively. The *color codes*(in connection with the *right vertical bars*) indicate the intensity (**a**), or the FWHM (**b**) of the absorption peaks of the proposed structure, respectively

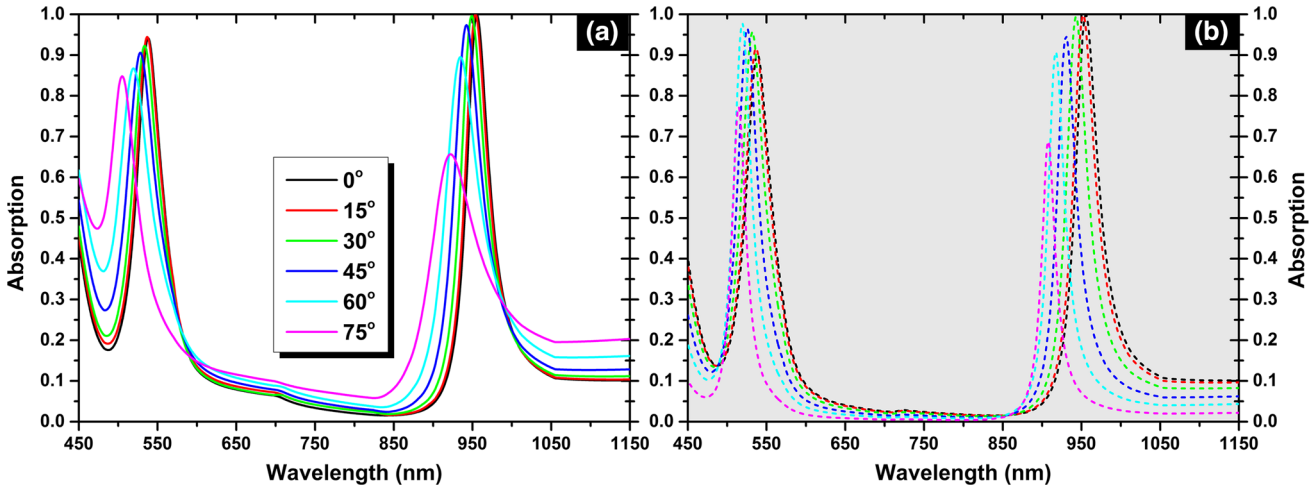

Fig. 4 Absorption spectra based on simulations for both transverse magnetic (TM) (**a** *solid lines*) and transverse electric (TE) (**b** *dashed lines*) polarizations and for different angles of incidence, varying from 0° to 75°

As already reported [11, 12], several MIM structures can be cascaded, to get a multiband light absorber. Indeed, we studied multilayer MIM structures to achieve multiband perfect absorption; Fig. 5 depicts the simulations for two layers of MIM structures, indicating the desirable thickness of TiO_2 dielectric layers as a function of the wavelength for absorption to occur at a level higher than 90% (a), and FWHM of the absorption peaks with intensity higher than 90% (b), respectively. In the 2-layered MIM structures, the overall bottom gold layer had a thickness of 150 nm, all the TiO_2 layers had a thickness of ~150 nm, while the middle and top gold layers had a thickness of 15–20 nm.

As can be seen in Fig. 5, if one sets the thickness of the intermediate metallic layer of the proposed double-layered MIM structure to 15 nm (with the top metallic cap being 20 nm), and keeps the sample thickness for both of the TiO_2 spacers at 110–150 nm, the resulting absorption peaks at ~550, ~600 and ~1000 nm will have an intensity of ~1.0 (see Fig. 5a) and a FWHM of ~45–50 nm (see Fig. 5b). On the other hand, if both of the TiO_2 spacers have a thickness of ~30 nm, the resulting absorption peaks are centered at ~500 and ~650 nm, respectively, with an intensity of ~0.98–1.0 and a FWHM of ~65–70 nm.

Following the above idea for achieving as broadband absorption as possible, we show in Fig. 6 the absorption spectra based on theoretical calculations of a 5-layered MIM structure, under normal EM wave incidence, while the corresponding spectrum of a single MIM structure of Fig. 2 is also presented, for comparison reasons.

As one can notice in Fig. 6, if we transform the simple MIM structure presented in Fig. 1 to a 5-layer one, as presented in the inset of Fig. 6, the absorption peak of a single MIM structure centered at ~550 nm (see Fig. 2 and

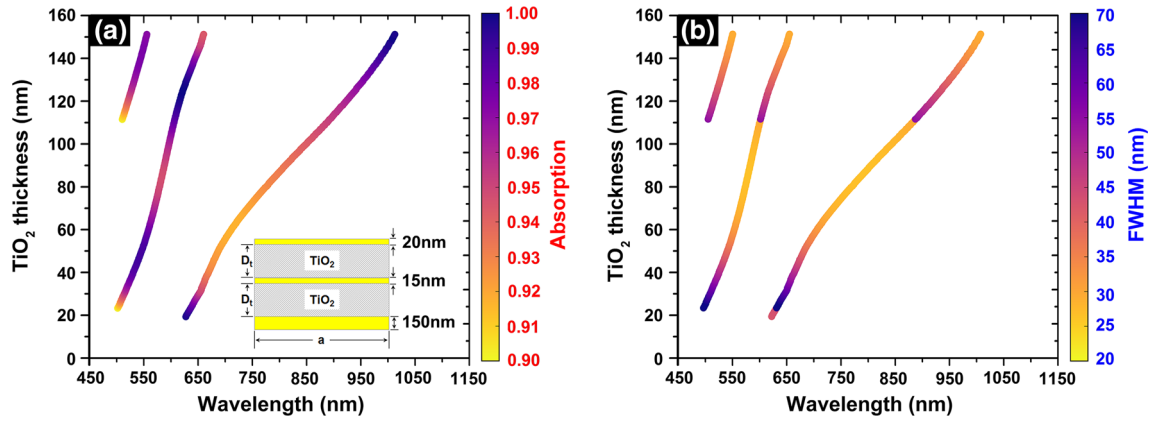

Fig. 5 Simulations of two MIM structures, indicating the desirable thickness of TiO_2 dielectric layers as a function of the wavelength for absorption to occur at a level higher than 90% (**a**), and FWHM of the absorption peaks with intensity higher than 90% (**b**), respectively. The *color codes* (in connection with the *right vertical bars*) indicate the intensity (**a**), or the FWHM (**b**) of the absorption peaks of the proposed structure, respectively

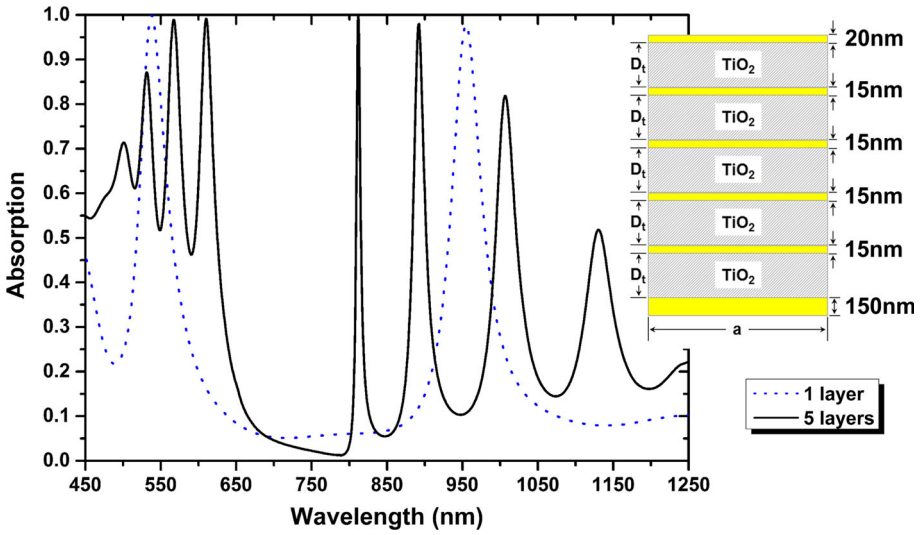

Fig. 6 Absorption spectra of 1-layered (*blue dotted line*), and 5-layered (*black solid line*) MIM perfect absorbers for normal EM wave incidence. In the *inset* of this figure, one can see the thickness of each metal layer, while $D_t = 150$ nm

dotted line in Fig. 6) will be transformed to a substantially broader, though oscillating, absorption peak at ~475–625 nm reaching a ~100% maximum intensity, indicating that indeed broadband absorption (in spite the amplitude oscillations) has been achieved.

4 Conclusions

In this work, we have demonstrated, both theoretically and experimentally, a perfect absorber in the visible region based on a MIM structure of proper geometric dimensions, for both TE and TM incident polarization, and for angles of incidence up to 75°. We have provided evidence that the single (and sharp) resonant absorber can be transformed to a substantially broader one, by simply building several layers of the proposed MIM structure, while no nanofabrication steps are required, and thus, the absorber can easily be made to cover a large area. The highly efficient absorption characteristics of the proposed structures can be potentially deployed for solar cells, optical filter elements, etc.

Acknowledgements This work was supported by the European Research Council under ERC Advanced Grant No. 320081 (PHOTOMETA). Work at Ames Laboratory was partially supported by the Department of Energy (Basic Energy Sciences, Division of Materials Sciences and Engineering) under Contract No. DE-AC02-07CH11358.

References

1. Y. Rádi, C.R. Simovski, S.A. Tretyakov, Phys. Rev. A **3**, 037001 (2015)
2. Y. Cui, Y. He, Y. Jin, F. Ding, L. Yang, Y. Ye, S. Zhong, Y. Lin, S. He, Laser Photonics Rev. **8**, 495–520 (2014)
3. T.V. Teperik, F.J.G. de Abajo, A.G. Borisov, M. Abdelsalam, P.N. Bartlett, Y. Sugawara, J.J. Baumberg, Nat. Photonics **2**, 288–301 (2008)

4. C. Wu, B. Neuner, J. John, A. Milder, B. Zollars, S. Savoy, G. Shvets, J. Opt. **14**, 024005 (2012)
5. H. Deng, T. Wang, J. Gao, X. Yang, J. Opt. **16**, 035102 (2014)
6. N.I. Landy, C.M. Bingham, T. Tyler, N. Jokerst, D.R. Smith, W.J. Padilla, Phys. Rev. B **79**, 125104 (2009)
7. S. Chou, P. Krauss, P. Renstrom, J. Vac. Sci. Technol. B **14**, 4129–4133 (1996)
8. L. Meng, D. Zhao, Q. Li, M. Qiu, Opt. Express **21**, A111 (2013)
9. D. Chanda, K. Shigeta, T. Truong, E. Lui, A. Mihi, M. Schulmerich, P.V. Braun, R. Bhargava, J.A. Rogers, Nat. Commun. **2**, 479 (2011)
10. C. Yang, W. Shen, Y. Zhang, D. Zhao, X. Liu, Opt. Commun. **331**, 310 (2014)
11. M. Yan, J. Opt. **15**, 025006 (2013)
12. G. Kájtar, M. Kafesaki, E.N. Economou, C.M. Soukoulis, J. Phys. D **49**, 055104 (2016)
13. A. Rampaul, I.P. Parkin, S.A. O'Neill, J. DeSouza, A. Mills, N. Elliott, Polyhedron **22**, 35–44 (2003)
14. G. Kenanakis, D. Vernardou, N. Katsarakis, Catal. Today **240**, 146–152 (2015)
15. P.B. Johnson, R.W. Christy, Phys. Rev. B **6**, 4370–4379 (1972)
16. E.D. Palik (ed.), *Handbook of Optical Constants of Solids* (Academic Press, Cambridge, 1997)
17. G. Kenanakis, N. Katsarakis, J. Environ. Chem. Eng. **2**, 1748–1755 (2014)
18. L. Miao, S. Tanemura, S. Toh, K. Kaneko, M. Tanemura, J. Cryst. Growth **264**, 246–252 (2004)
19. Y. Ohya, J. Mishina, T. Matsuda, T. Ban, Y. Takahashi, J. Am. Ceram. Soc. **82**, 2601–2606 (1999)
20. Y. Takahashi, Y. Matsuoka, J. Mater. Sci. **23**, 2259–2266 (1988)
21. H. Yu, J. Yu, B. Cheng, M. Zhou, J. Solid State Chem. **179**, 349–354 (2006)
22. H. Kocer, S. Butun, Z. Li, K. Aydin, Sci. Rep. **5**, 8157 (2014)
23. K. Bhattarai, Z. Ku, S. Silva, J. Jeon, J.O. Kim, S.J. Lee, A. Urbas, J. Zhou, Adv. Opt. Mater. **3**, 1779 (2015)
24. J. Jeon, K. Bhattarai, D.-K. Kim, J.O. Kim, A. Urbas, S.J. Lee, Z. Ku, J. Zhou, Sci. Rep. **6**, 36190 (2016)